# TWO WIRE RHOMBIC ILLUMINATOR PERFORMANCE AS PREDICTED BY THEORETICAL AND NUMERICAL MODELS

J. Patrick Donohoe*
Saad N. Tabet**
Clayborne D. Taylor*

*Department of Electrical and Computer Engineering
Mississippi State University
Mississippi State, Mississippi 39762

**Department of Electrical Engineering
FAMU/FSU College of Engineering
Tallahassee, Florida 32316-2175

## ABSTRACT

*The two wire rhombic illuminator (RI) is a rhombic wire antenna located over a ground plane which is used to generate near uniform electromagnetic fields over a specified working volume located below the antenna. The RI can be modeled as a simple two-wire transmission line at low frequencies but the transmission line model becomes inadequate at higher frequencies due to the enhanced radiation properties of the antenna. The performance of the RI including radiation effects is evaluated numerically using the Numerical Electromagnetics Code (NEC-2) and compared to that of the transmission line model. The antenna in the presence of a perfectly conducting ground plane is analyzed at frequencies ranging from 1MHz to 500MHz. Various segmentation schemes are utilized in order to accurately predict the performance of the RI at frequencies where the dimensions of the structure are very large in terms of wavelength.*

## INTRODUCTION

The rhombic transmission line configuration has received much attention in recent years as an illuminator for surveillance testing of electromagnetic shielding. The first detailed study of such an illuminator was performed by Baum [1] and Shen and King [2,3,4]. The uniformity of the working volume fields for the two-wire rhombic illuminator were analyzed by Zuffada and Engheta [5] using a two-wire transmission line operating in the TEM mode. As noted in [5], the accuracy of the transmission line model diminishes as the frequency is increased due to the appearance of longitudinal modes.

In this paper, the validity of the RI transmission line model is investigated using a numerical solution technique. An illustration of the RI over a perfectly conducting ground plane is shown in Figure 1. The actual RI dimensions and working volume location are shown in Figure 2. All wires have a diameter of 3.175mm. The antenna current and the individual components of the working volume electric field are computed over a range of 1MHz to 500MHz. Several aspects of the RI performance are noted with regard to the behavior of the antenna currents and working volume fields with frequency.

The RI may be driven in the common-mode (push-push) configuration with respect to the ground plane. The four wires of the RI are denoted as wire #1 and wire #3 (which make up the launch region) which are connected with wire #2 and wire #4, respectively, (which make up the termination region).

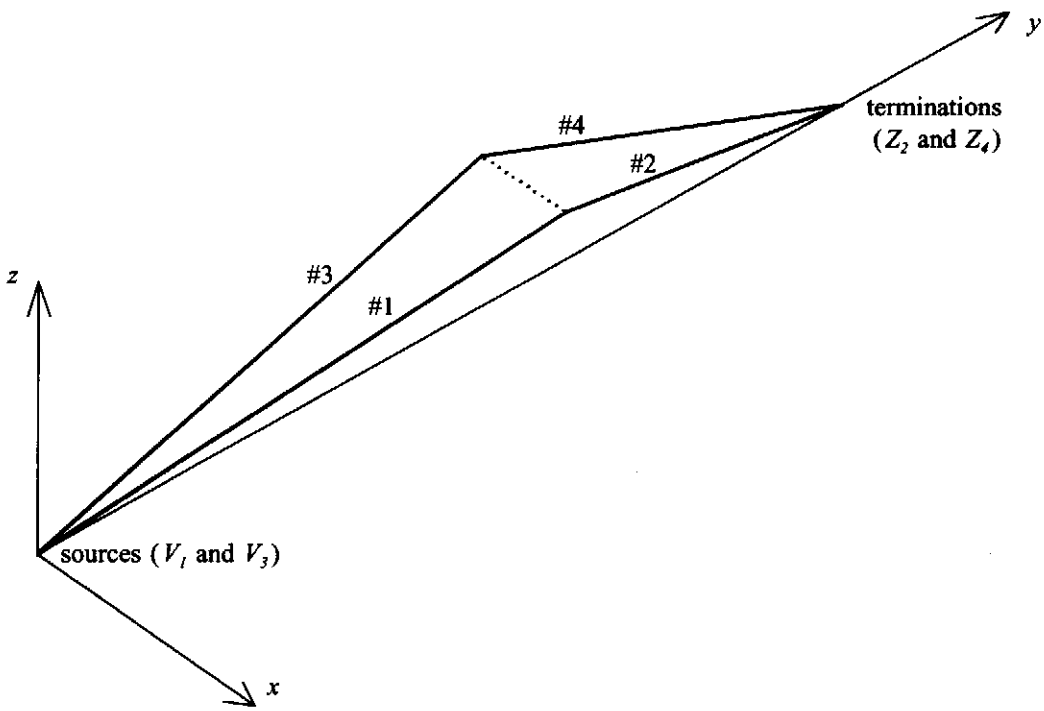


**Figure 1.** Rhombic illuminator (RI) wire configuration.

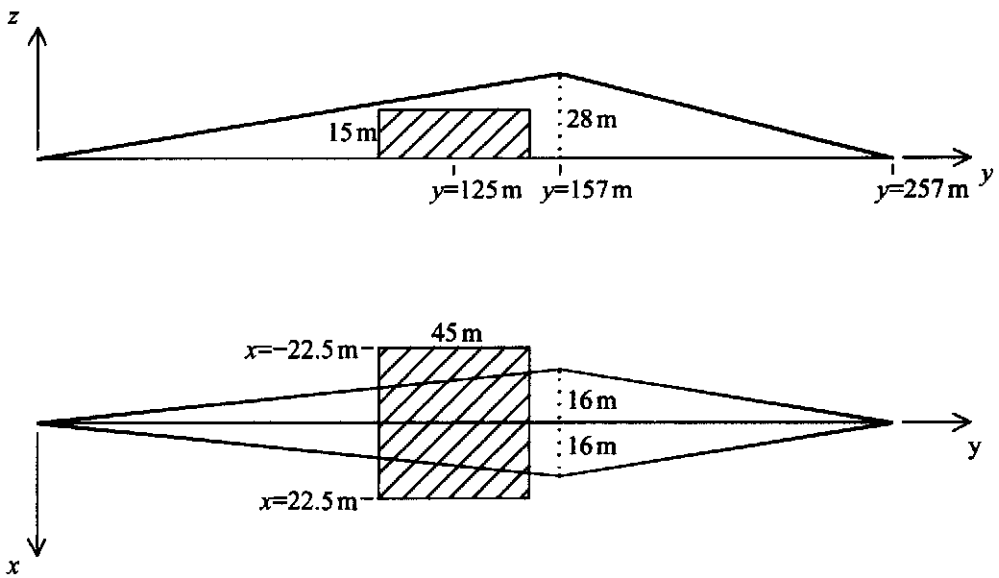


**Figure 2.** Rhombic illuminator and working volume dimensions.

The common mode excitation of the RI yields an electric field which is predominantly vertical in the given working volume.

## TRANSMISSION LINE MODEL OF THE RHOMBIC ILLUMINATOR

As previously mentioned, the RI may be modeled by a two-wire transmission line over a perfectly conducting ground plane at low frequencies. The TEM fields of the two-wire line under common-mode excitation are obtained by considering the static field of equivalent line charges over a perfectly conducting ground plane. For the given working volume dimensions, the values of the wire separation and wire height above ground may be optimized with regard to field uniformity [5].

The larger vertical component of the common-mode electric field is designated as the principal component while the smaller horizontal electric field component is referred to as the nonprincipal field component. The principal and nonprincipal fields ($E_z$ and $E_x$, respectively) for the common-mode excitation [5,8,9] are given by

$$E_z = \frac{q}{2\pi\varepsilon_o}\left[\frac{(z-b)}{(x-a)^2+(z-b)^2} + \frac{(z-b)}{(x+a)^2+(z-b)^2} - \frac{(z+b)}{(x-a)^2+(z+b)^2} - \frac{(z+b)}{(x+a)^2+(z+b)^2}\right] \tag{1}$$

*(Common-mode Principal Component)*

$$E_x = \frac{q}{2\pi\varepsilon_o}\left[\frac{(x+a)}{(x-a)^2+(z-b)^2} + \frac{(x-a)}{(x-a)^2+(z-b)^2} - \frac{(x+a)}{(x-a)^2+(z+b)^2} - \frac{(x-a)}{(x-a)^2+(z+b)^2}\right] \tag{2}$$

*(Common-mode Nonprincipal Component)*

where $q$ is the line charge density, $\varepsilon_0$ is the permittivity of vacuum, $2a$ is the distance between the wire centers and $b$ is the height of the wires above the ground plane. The value of the line charge density in (1) and (2) is related to the potential difference between each of the wires and ground ($V$) and the characteristic impedance of the common-mode two-wire line shown in Figure 3 as given by

$$\frac{q}{2\pi\varepsilon} = 30\frac{V}{Z_{cm}} \tag{3}$$

The characteristic impedance of the two-wire line ($Z_{cm}$) under common-mode excitation is

$$Z_{cm} = \frac{\eta_o}{4\pi}\left\{\ln\left[\frac{1+\left[1+(r/b)^2\right]^{1/2}-(r/b)}{1-\left[1+(r/b)^2\right]^{1/2}+(r/b)}\right]+\frac{1}{2}\ln\left[1+(b/a)^2\right]\right\} \tag{4}$$

where $\eta_0$ is the intrinsic impedance of vacuum and $r$ is the radius of the wires.

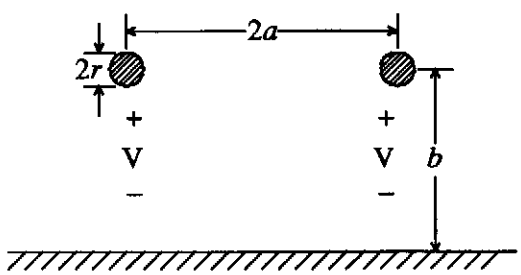


**Figure 3.** Common-mode two wire line over ground.

The principal and nonprincipal transverse electric fields in the working volume of the RI are symmetric about the $y$-$z$ plane given common-mode excitation. Therefore, the field behavior over the entire transverse cross-section of the working volume given by $[-22.5\,\text{m} \le x \le 22.5\,\text{m}]$ and $[0 \le z \le 15\text{m}]$ is evident given the fields over the cross-section defined by $[0 \le x \le 22.5\,\text{m}]$ and $[0 \le z \le 15\,\text{m}]$. The transverse cross-section located at the center of the working volume ($y$=125 m) is designated as $S_{wv}$ and is shown in Figure 4. For purposes of comparison, the individual electric field components are plotted over $S_{wv}$. The dimensions of the RI at $y$=125 m are $2a$=25.48 m (wire separation) and $b$=20.70 m (wire height above the ground plane).

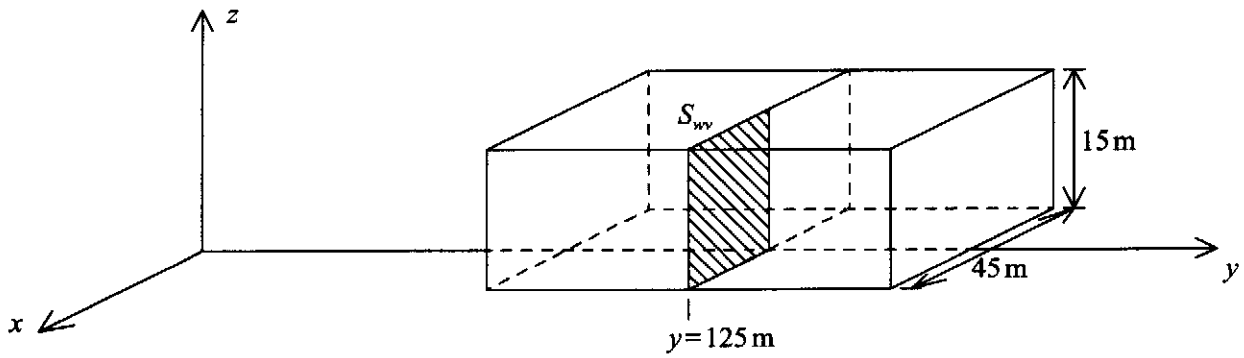


**Figure 4.** Working volume cross-sectional surface ($S_{wv}$) over which fields are plotted.

The transverse electric field components of a similarly spaced two-wire transmission line over a ground plane ($2a$=25.48 m, $b$=20.70 m, $r$=1.5875 mm) with $V$=1 V are shown in Figures 5 and 6. The principal electric field component of the transmission line model shown in Figure 5 contains a broad peak along the upper edge of the working volume ($z$=15 m) which corresponds to points directly below the transmission line conductor. The principal electric field is relatively uniform over the remainder of the working volume. The nonprincipal electric field component shown in Figure 6 is zero-valued along the lower edge of the working volume (tangent to the ground plane) and increases in magnitude as the observation point is moved away from the ground plane. The nonprincipal electric field contains a null along the upper edge of the working volume which corresponds to the point where the horizontal components due to both wires and their images cancel one another. The $x$-coordinate of this null lies between the transmission line center point at $x$=0 and the coordinate of the transmission line conductor at $x=a$. The transverse fields of the transmission line model are compared to the fields generated by the corresponding *NEC* thin-wire model of the RI described in the following section.

## NUMERICAL MODEL OF THE RHOMBIC ILLUMINATOR

The number of segments required to model each of the four wires of the RI using *NEC-2* is based on the frequency of operation. In general, the segment lengths should be chosen in the range of 0.001λ to 0.1λ to maintain numerical stability [6]. This segment length requirement makes the analysis of electrically long thin-wire structures (such as the RI at high frequencies) computationally prohibitive. However, the segment lengths can be exponentially graded over the entire wire ("entire grading") or a portion of each wire ("partial grading") [7,8,9] to minimize the number of segments required for an accurate solution of the RI geometry. These segmentation schemes allow for electrically short segments in critical regions (source, termination, wire bends) while allowing for longer segments over the remainder of the structure.

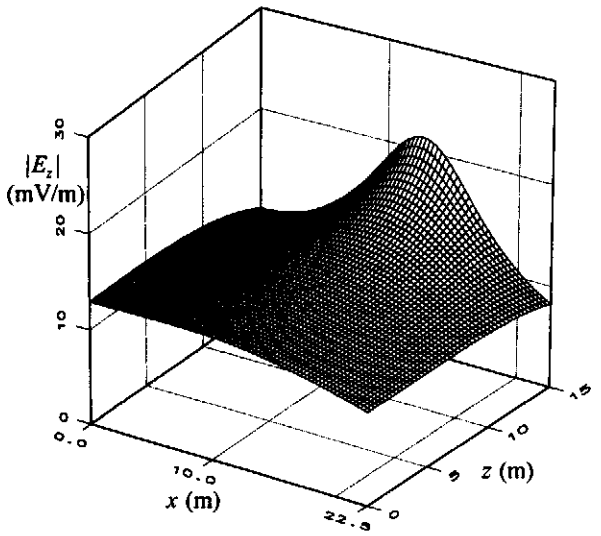


**Figure 5.** Principal transverse electric field magnitude on $S_{wv}$ (transmission line model).

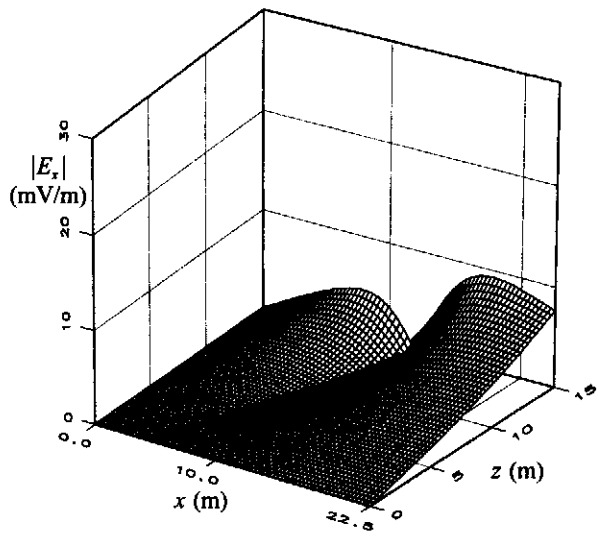


**Figure 6.** Nonprincipal transverse electric field magnitude on $S_{wv}$ (transmission line (model).

The segments on the launching region wires (#1 and #3) are numbered from the ground plane to the apex of the RI. That is, the first segment on each launch wire is connected to the ground plane while the last segment is connected to the termination wire at the apex. The segments on the termination region wires (#2 and #4) are numbered from the apex to the ground plane. The two common-mode voltage sources (applied electric-field sources), $V_{S1}$ and $V_{S2}$, are placed on the second segment of wire #1 and wire #3, respectively. The magnitude of both voltage sources is one volt with a phase of zero degrees. The terminations placed on the last segments of wire #2 and wire #4 are lumped resistive loads of 630Ω. The 630Ω lumped resistive value corresponds to twice the average common-mode characteristic impedance along the length of the RI as given in Equation (4).

*NEC* allows for the utilization of structural symmetry to simplify the geometry input as well as the solution process. The RI configuration shown in Figure 1 is symmetric about the *y-z* plane. Thus, using symmetry, only wire #1 and wire #2 are needed to describe the entire RI structure. The voltage sources are not reflected using symmetry so that both sources of the RI must be defined explicitly. *NEC* does, however, allow for the reflection of loaded segments so that the resistively-loaded segment on wire #2 is automatically reflected to wire #4 using symmetry.

The previously defined thin-wire model of the RI is analyzed using discrete *NEC* models over a frequency range of 1 MHz to 500 MHz. The *NEC* models developed for the RI are highly sensitive to the frequency of operation because of the critical nature of the segment length with regard to wavelength. For this reason, the RI model is analyzed at five distinct frequencies: 1 MHz, 10 MHz, 100 MHz, 300 MHz and 500 MHz. The RI current and electric field components over $S_{wv}$ are computed at each frequency. The total number of unknowns ($N_{total}$) is equal to the total number of segments required to model a symmetric cell (wire #1 plus wire #2). Within *NEC*, the maximum array dimension with regard to the number of segments must be $2N_{total}$. The total length of the RI symmetric cell is approximately 265 m. The total electrical lengths of the RI symmetric cell at the various frequencies of interest are listed in Table 1.

The RI at 1 MHz is easily modeled with "optimum" length segments of 0.01λ. The length of 0.01 λ lies one order of magnitude above the recommended minimum segment length and one order of magnitude below the maximum recommended segment length. Wire #1 and wire #2 are divided into equal segments

of length approximately 0.01λ which yields 54 segments on wire #1 and 35 segments on wire #2 for a total of 89 segments in a symmetric cell.

The total length of wire #1 plus wire #2 at 10MHz is approximately 8.8λ. Thus, approximately 880 segments would be required to model the RI with 0.01λ segments. Yet, the use of this many segments yields a solution which is unnecessarily lengthy. The accuracy of the *NEC* model for long straight wires is not appreciably affected by using segments which are longer than 0.01λ away from the critical regions of the structure [6]. Thus, by exponentially grading the segments along the RI wires, the total number of segments required can be reduced significantly. The segments near the source must be short and of comparable length to yield accurate representations of the applied electric field sources. Therefore, the first segment on wire #1 is chosen to be 0.01λ in length. The partial grading technique is then used with a grading factor of 1.1 (10% increase in length from segment to segment) until the segments reach a maximum length of $\Delta_{max}=0.1\lambda$. The same segment grading is used at the apex end of wire #1. The remaining midsection of wire #1 is modeled with uniform length segments of length $\Delta_{max}$. The same segmentation scheme is applied to the termination wire (wire #2) resulting in 83 segments on wire #1 and 65 segments on wire #2 for a total of 148 segments.

At 100MHz, the total electrical length of the symmetric cell is approximately 88λ. In order to significantly reduce the number of segments required at this frequency, the partial grading scheme must be employed. As in the 10MHz case, the shortest segments on wire #1 and wire #2 are defined with lengths of 0.01λ and a grading factor of 1.1 is used for the weighted portions of the wires. The maximum segment length is chosen to be $\Delta_{max}=0.2\lambda$. This segmentation results in 310 segments on wire #1 and 218 segments on wire #2 which yields $N_{total}=528$.

The total electrical length of the symmetric cell at 300MHz is approximately 264λ. The same segmentation scheme as outlined for the 10MHz and 100MHz cases is used for the 300MHz case. The grading factor is again chosen to be 1.1 while the maximum segment length is chosen as 0.3λ. The resulting segment totals on wire #1 and wire #2 are 585 and 400, respectively. Thus, the total number of segments in the symmetric cell is 985.

The previously defined segmentation scheme is applied to the RI at 500MHz. The electrical length of the RI symmetric cell at 500MHz is in excess of 440λ. A grading factor of 1.1 and a maximum segment length of 0.4λ are utilized. This model of the RI yields 724 segments on wire #1 and 493 segments on wire #2. Thus, the entire symmetric cell requires a total of 1217 segments.

The characteristics of the five *NEC* models are summarized in Table 1. The use of *NEC* models which contain segment lengths in excess of 0.1λ requires special consideration with regard to the interaction approximation distance within *NEC*. When segments are separated by more than a prescribed distance (known as the interaction approximation distance), the source segment is modeled as an infinitesimal current element at the segment center. This approximation is accurate when using short segments. However, longer segments may have significant variation of current magnitude and phase along the length of the segment which makes this approximation inaccurate. Thus, when using longer segments, the interaction approximation must not be utilized. The interaction approximation distance may be defined by the user but a default value of 1m is assumed in *NEC*. In the results given here, the interaction approximation distance is defined large enough that the interaction approximation is not implemented.

## NUMERICAL RESULTS FOR THE THIN-WIRE RI MODEL

The magnitude of the resulting current along wire #1 and wire #2 of the RI is shown in Figure 7. The current magnitude at 1MHz exhibits a standing wave pattern that is very slightly damped along the length of the two wires. The principal transverse, nonprincipal transverse and longitudinal components of the electric field over $S_{wv}$ are shown in Figures 8, 9 and 10, respectively. The transverse electric field plots may be compared with those of the two-wire transmission line (Figures 5 and 6). As expected, the general distribution of transverse electric field components are nearly identical to those of the two-wire

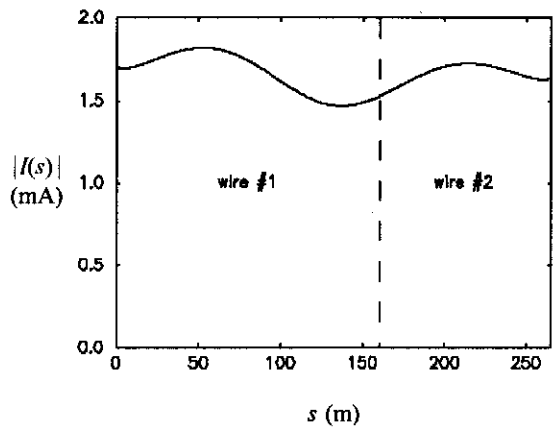


**Figure 7.** RI current magnitude on wires #1 and #2 at 1 MHz.

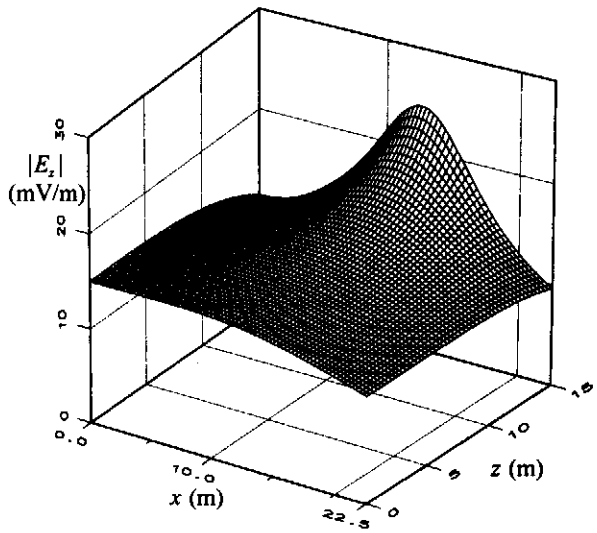


**Figure 8.** Principal transverse electric field magnitude on $S_{wv}$ at 1 MHz.

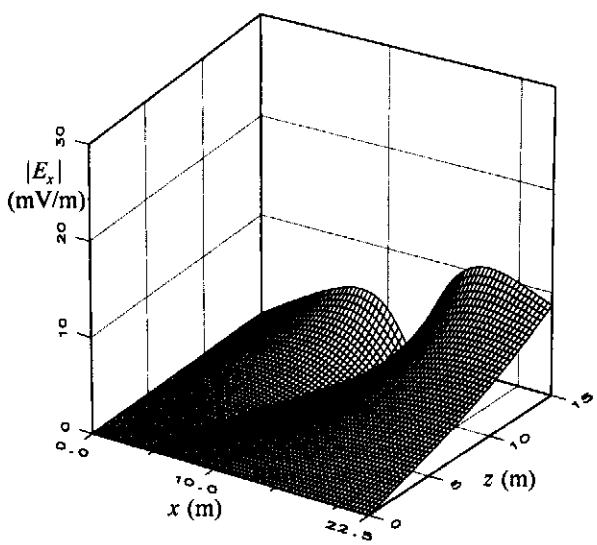


**Figure 9.** Nonprincipal transverse electric field magnitude on $S_{wv}$ at 1 MHz.

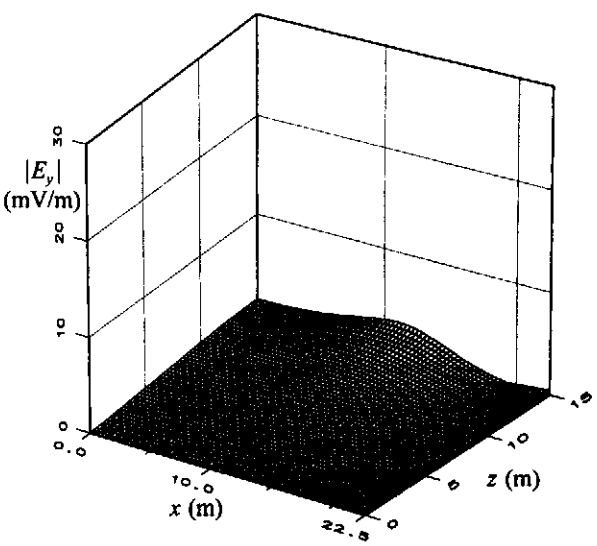


**Figure 10.** Longitudinal electric field magnitude on $S_{wv}$ at 1 MHz.

| $f$ (MHz) | Total length (wire #1 + wire #2) | Segment grading scheme | $\Delta_{max}$ | $N_{total}$ |
|---|---|---|---|---|
| 1 | 0.8822λ | none | 0.01λ | 89 |
| 10 | 8.822λ | partial | 0.1λ | 148 |
| 100 | 88.22λ | partial | 0.2λ | 528 |
| 300 | 264.7λ | partial | 0.3λ | 985 |
| 500 | 441.1λ | partial | 0.4λ | 1217 |

**Table 1.** Descriptions of the RI *NEC* models.

transmission line TEM mode. The magnitudes of the transverse electric field components for the RI model are slightly higher than the corresponding transmission line values. The magnitude of the longitudinal electric field component is small in comparison with the transverse components.

The magnitude of the current along wires #1 and #2 of the RI at 10MHz is plotted in Figure 11. The corresponding electric field components are plotted over $S_{wv}$ and appear in Figures 12, 13 and 14. The magnitude of the RI source current at 10MHz exhibits a significant increase when compared to the 1MHz value. Yet, the RI current at 10MHz exhibits a slightly higher rate of decay than the 1MHz distribution. The general shapes of the electric field components, both transverse and longitudinal, remain unchanged from the 1MHz values. The magnitudes of all three electric field components at 10MHz are slightly larger than the corresponding 1MHz values.

The 100MHz RI current magnitude is shown in Figure 15. The resulting 100MHz working volume electric field components are given in Figures 16, 17 and 18. An increase in the magnitude of the source current from 10MHz to 100MHz is observed. However, the damping factor of the 100MHz current is larger than that of the 10MHz current yielding only slightly higher values of current magnitude in the vicinity of the working volume (near the wire apex). The magnitudes of both the transverse and longitudinal components of the working volume electric field exhibit a slight increase over the corresponding values at 10MHz. The variation in the working volume field components with respect to wavelength becomes apparent at 100MHz as shown in Figures 16, 17 and 18.

The current magnitude along the RI wires at 300MHz is plotted in Figure 19, while the corresponding electric field components over $S_{wv}$ are plotted in Figures 20, 21 and 22. A general trend is evident in the variation of the RI current and working volume field values as a function of frequency. As the frequency of operation is increased, the source current magnitude is increased. The standing wave pattern along the RI wires stays relatively constant with frequency. The resulting working volume electric field components exhibit a small increase in magnitude as the frequency is increased.

The magnitude of the current on wires #1 and #2 of the RI at 500MHz is shown in Figure 23. The electric field components in the working volume of the RI at 500MHz are shown in Figures 24, 25 and 26. The current magnitude at the source is slightly larger than that of the 300MHz case but the current distribution away from the source is quite similar to that of the 300MHz case. The standing wave amplitude is slightly higher than that of the 300MHz case. The working volume field components exhibit a small increase in amplitude over the 300MHz case as expected.

In order to test the convergence of the previous *NEC* solutions when using relatively long segments, the 300MHz and 500MHz cases are modeled with slightly shorter segments and the resulting currents are compared with the currents obtained with the initial models. These comparisons are shown in Figures 27 and 28. For both the 300MHz and 500MHz cases, the current distributions are quite similar with only minor variations in the standing wave amplitude.

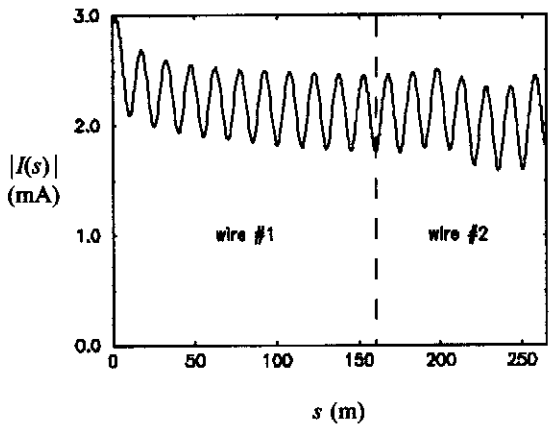


**Figure 11.** RI current magnitude on wires #1 and #2 at 10 MHz.

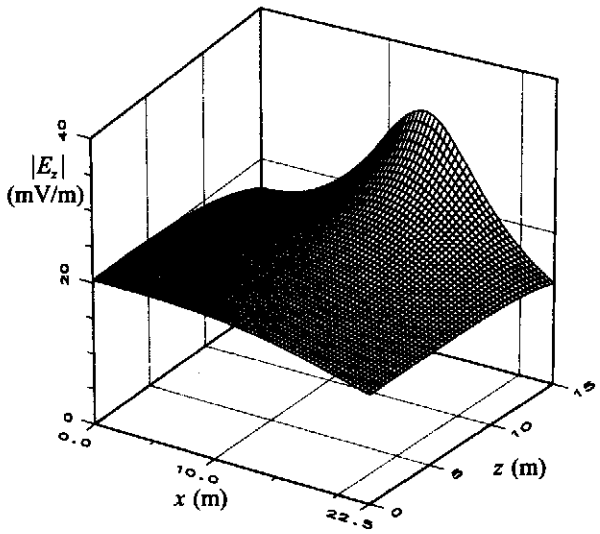


**Figure 12.** Principal transverse electric field magnitude on $S_{wv}$ at 10 MHz.

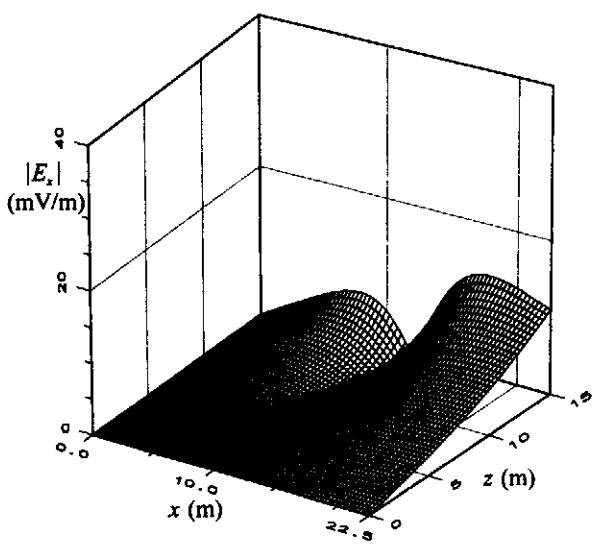


**Figure 13.** Nonprincipal transverse electric field magnitude on $S_{wv}$ at 10 MHz.

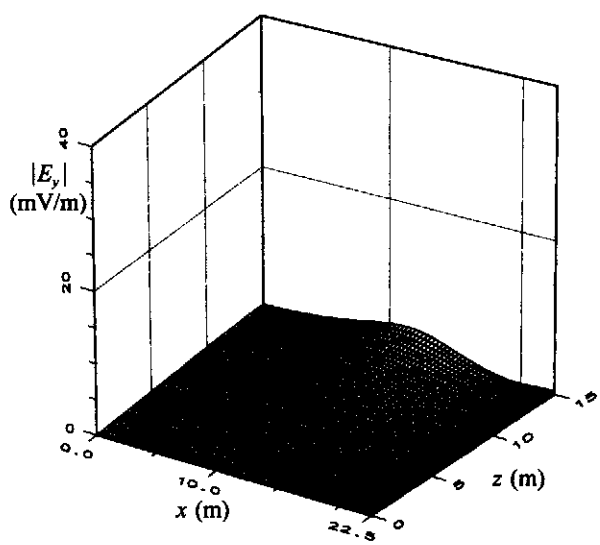


**Figure 14.** Longitudinal electric field magnitude on $S_{wv}$ at 10 MHz.

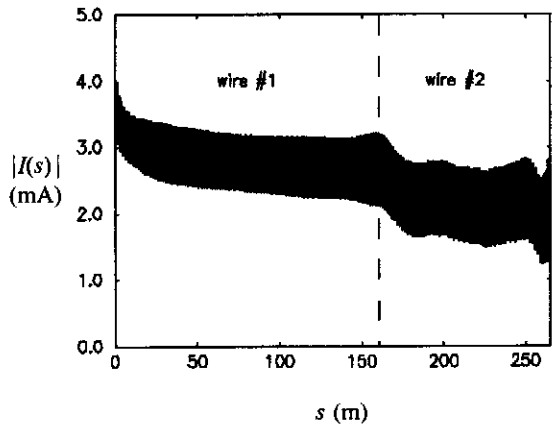


**Figure 15.** RI current magnitude on wires #1 and #2 at 100 MHz.

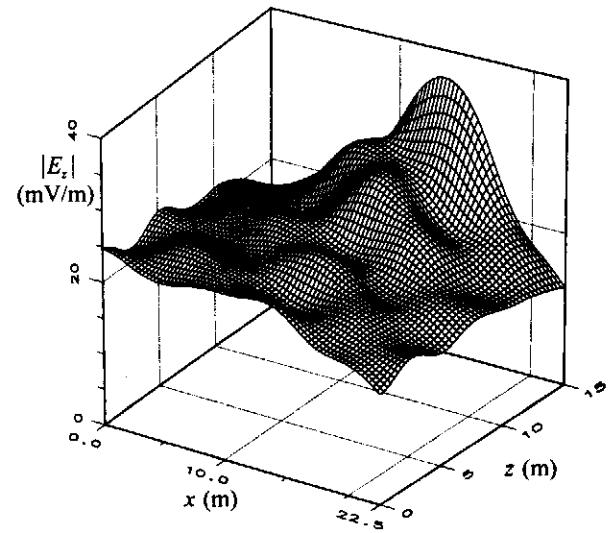


**Figure 16.** Principal transverse electric field magnitude on $S_{wv}$ at 100 MHz.

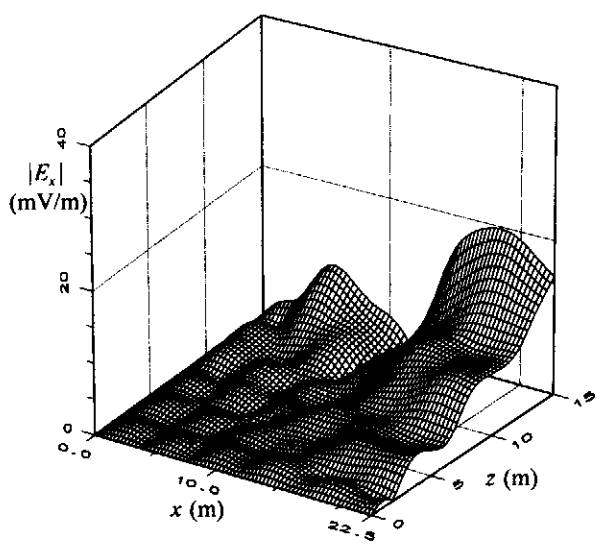


**Figure 17.** Nonprincipal transverse electric field magnitude on $S_{wv}$ at 100 MHz.

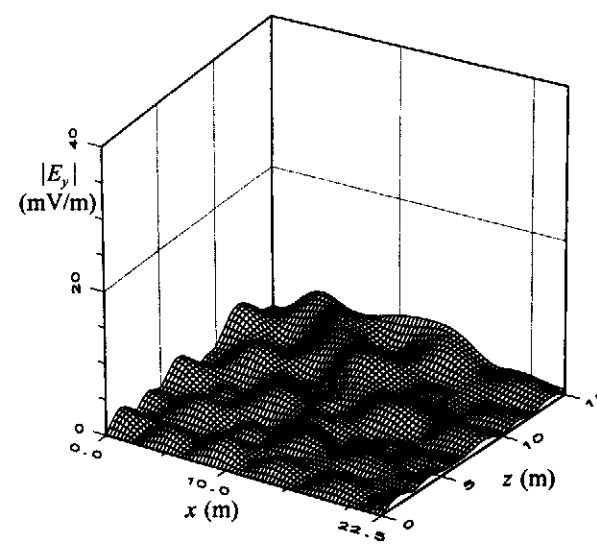


**Figure 18.** Longitudinal electric field magnitude on $S_{wv}$ at 100 MHz.

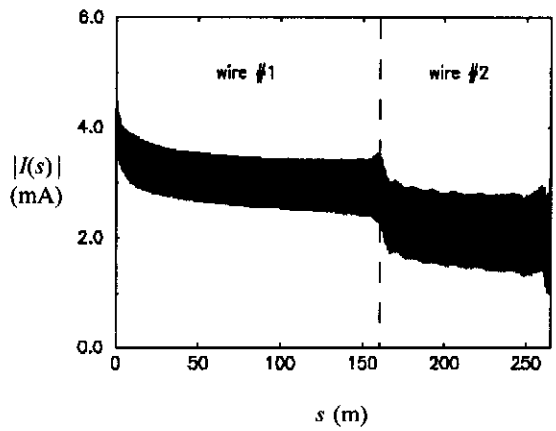


**Figure 19.** RI current magnitude on wires #1 and #2 at 300 MHz.

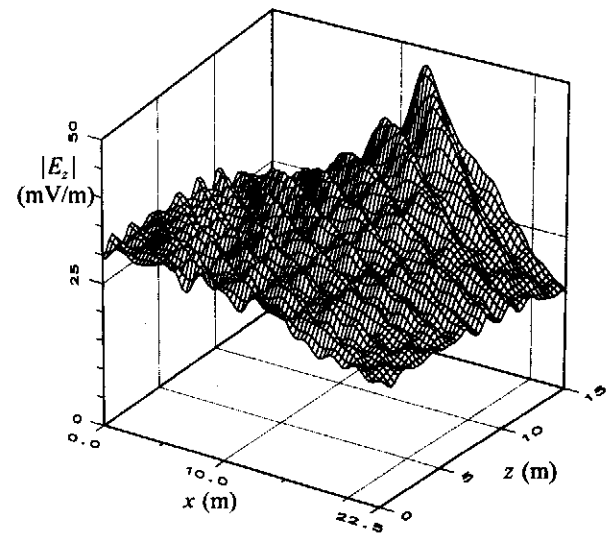


**Figure 20.** Principal transverse electric field magnitude on $S_{wv}$ at 300 MHz.

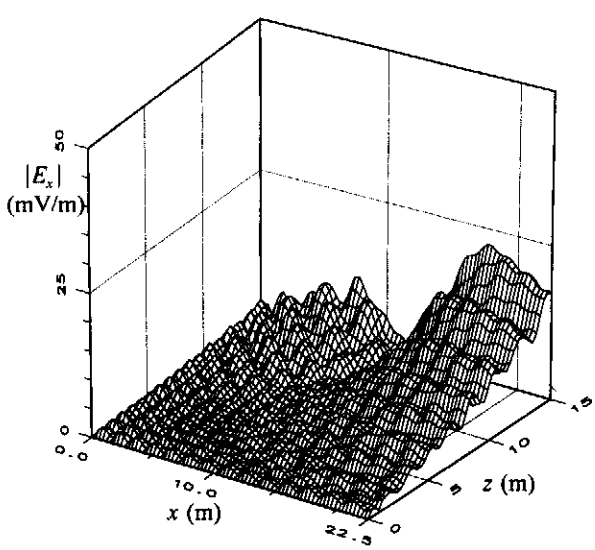


**Figure 21.** Nonprincipal transverse electric field magnitude on $S_{wv}$ at 300 MHz.

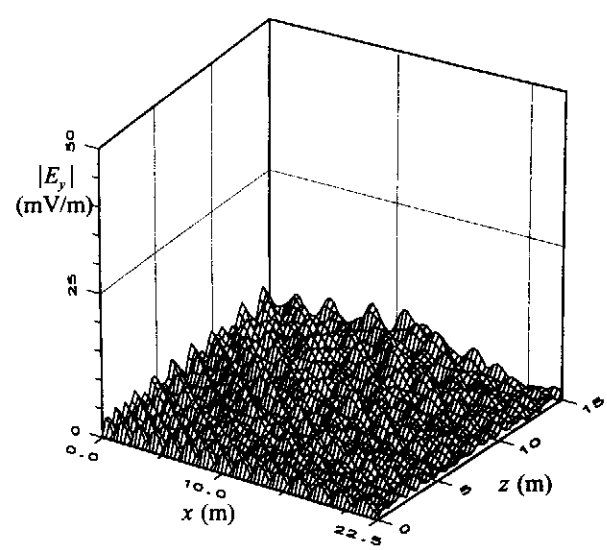


**Figure 22.** Longitudinal electric field magnitude on $S_{wv}$ at 300 MHz.

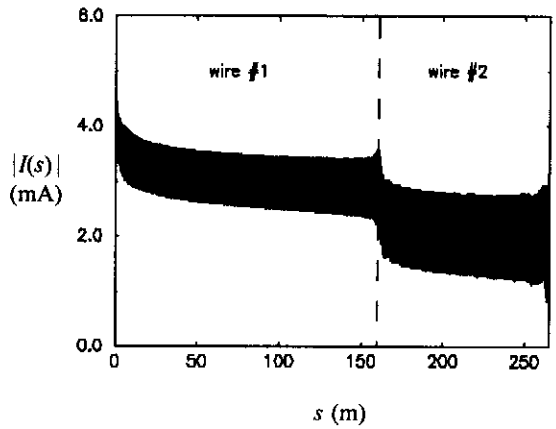


**Figure 23.** RI current magnitude on wires #1 and #2 at 500 MHz.

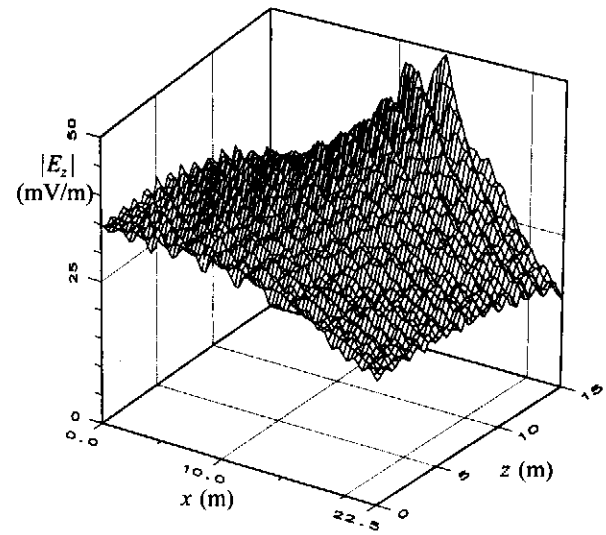


**Figure 24.** Principal transverse electric field magnitude on $S_{wv}$ at 500 MHz.

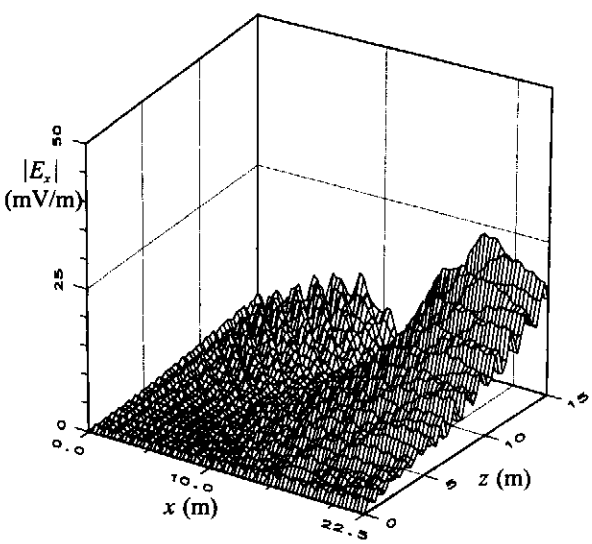


**Figure 25.** Nonprincipal transverse electric field magnitude on $S_{wv}$ at 500 MHz.

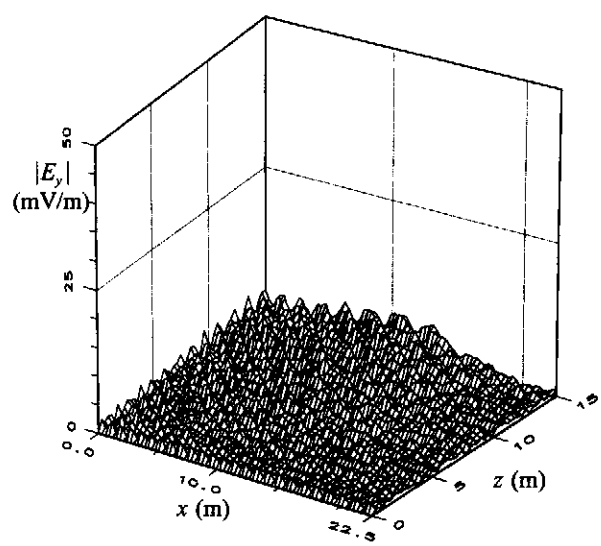


**Figure 26.** Longitudinal electric field magnitude on $S_{wv}$ at 500 MHz.

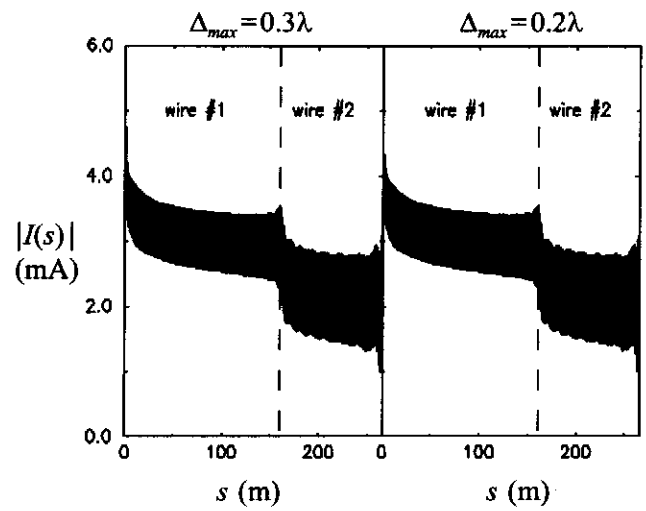


**Figure 27.** Comparison of RI current magnitude at 300MHz with $\Delta_{max}=0.3\lambda$ and $\Delta_{max}=0.2\lambda$

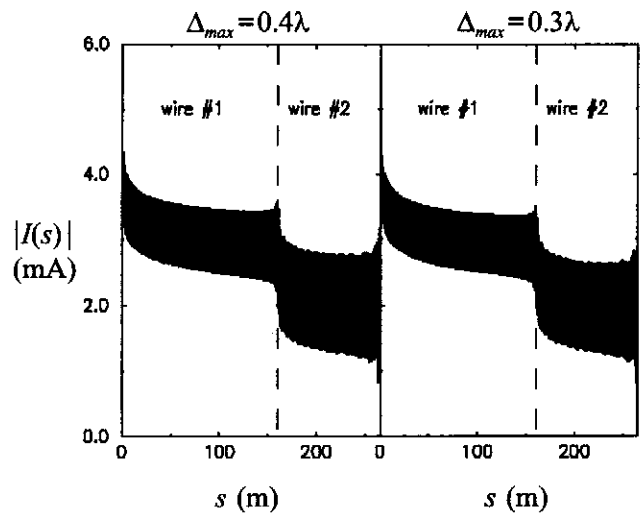


**Figure 28.** Comparison of RI current magnitude at 500MHz with $\Delta_{max}=0.4\lambda$ and $\Delta_{max}=0.3\lambda$

## ANALYSIS OF RESULTS AND CONCLUSIONS

The rhombic illuminator configuration has been analyzed using a numerical solution technique over the frequency range of 1MHz to 500MHz. The numerical solution is obtained using *NEC* with five discrete models at 1, 10, 100, 300 and 500MHz. The antenna current and the working volume electric field components were computed and compared to the fields obtained using the two-wire transmission line TEM model. The current along the wires of the illuminator was found to display several basic physical characteristics. The current exhibited a damped standing wave pattern which remains relatively constant over the frequency range of interest. Reflections from the wire bend become evident at frequencies of 100MHz and above. The current magnitude in the source region increases rapidly from 1 to 100MHz and at a slower rate at the higher frequencies. Overall, the average current magnitude along the RI wires is relatively constant over the given frequency range.

The electric field components in the working volume also exhibit several distinct characteristics. The magnitudes of the working volume fields increase with frequency since the peak currents on the antenna also increase with frequency. The general shapes of the field component distributions depend on the distribution of current on the illuminator wires. Since the current magnitude distribution is relatively constant over the frequency range of interest, the field component distributions also remain relatively constant. The magnitude of the longitudinal electric field component remains quite small in comparison to the principal transverse component indicating that no significant longitudinal modes are excited at frequencies of 500MHz and below. As shown in Figures 8, 12, 16, 20 and 24, the RI performance is satisfactory up to 500MHz with regard to the uniformity of the principal transverse field in the working volume. The transmission line model yields an accurate prediction of the general shape of the working volume transverse field component distributions but does not accurately predict the magnitudes of these fields [10]. At 500MHz, the transverse fields are roughly three times larger than those predicted by the theoretical model. It may be possible to reduce the standing wave amplitude along the structure at the various frequencies by improved load matching or through the use of distributed loading along the wires.

## REFERENCES


1. C. E. Baum, "Impedances and Field Distributions for Symmetrical Two Wire and Four Wire Transmission Line Simulators," *Sensor and Simulation Notes*, Note 27, AFWL, Kirtland AFB, June 1970.

2. H-M. Shen and R. W. P. King, "The Rhombic EMP Simulator," *IEEE Transactions on Electromagnetic Compatibility*, Vol. EMC-24, No. 2, pp. 255-265, May 1982.

3. H-M. Shen and R. W. P. King, "Experimental Investigation of the Rhombic EMP Simulator: Comparison with Theory and Parallel Plate Simulator," *IEEE Transactions on Electromagnetic Compatibility*, Vol. EMC-24, No. 3, pp. 349-355, August 1982.

4. H-M. Shen and R. W. P. King, "Theoretical Analysis of the Rhombic Simulator Under Pulse Excitation," *IEEE Transactions on Electromagnetic Compatibility*, Vol. EMC-25, No. 1, pp. 47-55, February 1983.

5. C. Zuffada and N. Engheta, "Field Uniformity Criteria for the Design of a Two-Wire EMP Simulator," *Electromagnetics*, Vol. 8, No. 1, pp. 29-35, 1988.

6. G. J. Burke and A. J. Poggio, "Numerical Electromagnetics Code (NEC) - Method of Moments," Vol. 2, Naval Ocean Systems Center, Technical Report NOSC TD 116, January 1981.

7. S. N. Tabet, J. P. Donohoe, and C. D. Taylor, "Using Nonuniform Segment Lengths with NEC to Analyze Electrically Long Wire Antennas," *Applied Computational Electromagnetics Society Journal*, Vol. 5, No. 2, pp. 2-16, Winter 1990.

8. S. N. Tabet, "High Frequency Performance of the Rhombic Illuminator," Doctoral Dissertation, Mississippi State University, December 1989.

9. J. P. Donohoe and S. N. Tabet, "HSI High Frequency Performance Verification/Upgrade," EG&G Projects, Final Technical Report, Contract No. F29601-88-0001, Subtask 03-05/00, November 1989.

10. B. D. Popovic, "Frequency-Domain Analysis of a Large NEMP-Simulator Wire Antenna," *IEE Proceedings*, Vol. 135, Pt. H, No. 2, April 1988.